Hindawi
Geofluids
Volume 2021, Article ID 6622214, 15 pages
https://doi.org/10.1155/2021/6622214

Research Article

Failure Analysis of a Highway Cut Slope with Anti-Slide Piles

Hongjie Chen,[1] Guangcheng Zhang,[2] Zheng Chang,[3] Lian Wen,[2] and Wentao Gao[3]

[1]*Huaneng Lancang River Hydropower Inc., Kunming, China*
[2]*China University of Geosciences, Wuhan, China*
[3]*China Highway Engineering Consulting Corporation, Wuhan, China*

Correspondence should be addressed to Guangcheng Zhang; zhangguangc@cug.edu.cn

Received 1 January 2021; Revised 30 January 2021; Accepted 10 February 2021; Published 3 March 2021

Academic Editor: Chun Zhu

Landslides induced by engineering construction are very common in reality; it is necessary to clarify the causes of landslide failure to avoid similar accidents. A landslide induced by highway construction is taken as a case. Field observations, data collection, and analyses were used to investigate the deformation and causes of the landslide. The failed slope is mostly comprised of gravel soil, there were some shear cracks on both sides of the slope before sliding, and most tensile cracks were connected with shear cracks after sliding. The cut slope of this highway was designed to be protected by prestressed anchor sheet piles. However, in the construction process, the slope in front of the antipiles was removed when the piles were constructed without any anchor cables, which led to the shear damage of a row of anti-slide piles with a 15-meter-long cantilever. Moreover, continuous rainfall over several days aggravated the landslide damage because of increase of the self-weight and degradation of the mechanical parameters of the slope materials. The mechanical and simulation analyses both show that the resistance provided by the cantilever piles was not enough to prevent the force behind the piles. The irrational construction process and rainfall caused the slope failure.

1. Introduction

The irrational construction process in the slope can lead to the deformation or even the destruction of nearby buildings or main works, threatening human safety. A series of external factors including earthquake, rainfall, ice and snow melt, and artificial disturbances can induce the deformation of slopes and form landslides [1–5]. Many cases of landslides induced by excavation, rainfall, groundwater, and earthquakes have been reported. A massive landslide that buried 83 people on March 29, 2013, in Tibet was triggered by thermal expansion and contraction stress induced by rainy and snowy melt. A massive landslide occurred in the Las Colinas neighbourhood of Santa Tecla, El Salvador, in Central America as a result of the M = 7.6 earthquake of January 13, 2001 [6]. A subdivision of 29 homes located in Lakeport, California, is being threatened by ground that is moving from a few inches to a few feet every day, which is caused by excess ground water.

In recent years, many studies on cut slope deformation and stability have been undertaken [7, 8]. The deformation failure modes of gravity retaining walls were summed up by applying near-field data in the Wenchuan earthquake and calculating the distribution of seismic earth pressure under different displacement modes [9]. Other scholars concentrated on landslide induced by rainfall. Harris et al. [10] showed that the cut slope failed due to the existence of a large number of dry cracks which intensified the rainwater infiltration. Chen and Cui [11] suggested that the inducing factor of the Wulipo landslide is hydrostatic and hydrodynamic pressure change caused by heavy continuous rainfall. Chatra et al. [12] carried out the numerical simulation method to study the effects of rainfall intensity and duration on pore pressure generation, saturation, slope stability, and shear strain increment. Zhang et al. [13] summarized the failure model as "instability-translational slide-tension fracture-collapse" and the formation mechanism as "translational landslide induced by heavy rainfall" of the landslide. Moreover, the failure mode and stability analysis of the cut slope are studied as the other problem. Singh et al. [14] established the relation between the structural discontinuities and surface

topography of cut rock slope and promoted the probable failure modes using the kinematics analysis method. Oh and Lu [15] expanded the traditional limit equilibrium and finite element methods with consideration of unsaturated conditions using a generalized effective stress framework and noted that the hydromechanical framework under the suction stress-based effective stress can reconcile the observed timing of failure. Da et al. [16] developed an experimental research programme to promote the parameter evaluation of soil from cut slopes and to assess the potential of the anthropic impact on the soil susceptibility to accelerated erosion process.

Slope excavation is routinely required to facilitate the highway, while the excavation affects the stability factor of the slope. The design process has to carefully address the potential impact of excavation on the surrounding environment. Here a landslide, induced by the irrational construction process of a cut slope and continuous rainfall, was analyzed from the deformation characteristics, influencing factors, to mechanical and numerical calculations.

2. Engineering Geological Conditions

The cut slope of the failed highway is located on the right side of the K19+060~K19+320 segment of this highway in Yanling County, Hunan Province. The highway in this segment is almost a straight line with a trend of nearly S15°E. The stratum is a monocline, and the dip direction of the bed rock is E5°N with a dip angle of 39°. Therefore, a dip slope is formed on the right side of the highway, and a reverse slope formed on the left at the same time.

The landform of the site belongs to an erosion midlow mountain. The ground elevation in this field is from 299.2 m to 328.8 m and is generally higher in the west than in the east. The surface slope is nearly 20°~35°. The mountain is steady and is well covered with plants. There are some v-shaped valleys.

The slope is composed of residual silty clay, Quaternary and siltstone gravel soil, and quartz sandstone of the Majian group in the Middle Devonian (D_2t) (shown in Figure 1). The soil and rock mass is as follows.

(1) Silty clay (1-4-1, Q^{el+dl}) is brown yellow or grey brown; its shape is angular or elliptical. It is hard plastic in general and contains some gravel and 0.2~3 cm breccia that originates from sandstone. The thickness of this layer is 0.80~3.70 m, and there are a few plant roots in the superficial layer approximately 0.60 m below the ground

(2) Gravel soil (1-4-2, Q^{el+dl}) is motley, slightly wet, and of slight or medium compactness. It consists of approximately 21 percent clay and sand. The particle size of gravel is generally 15~30 mm and is no more than 45 mm. The gravels are of medium psephicity, mainly subrounded and partially subangular. The thickness is approximately 6.0~20.40 m

(3) Strong weathered siltstone (7-1-2, D_2t) is grey or yellow and has a fine grained texture. The joints are developed, and the structures of the original rock have been mostly destroyed; therefore, it is easily softened and disintegrated when it meets water

(4) Moderate weathered siltstone (7-1-3, D_2t) is grey or light purple and has a medium layered structure and silty texture. The joints are also developed, and the drill holes show that most of the rock mass is stumpy and that only a small portion is columnar with a length of 5~20 cm and an rock quality designation (RQD) value of 21%-40%; some are broken into fragments

(5) Moderately weathered quartz sandstone (7-2-3, D_2t) is light grey and has a fine grained texture and massive structure. It belongs to hard rock mass. The drill core is mostly columnar and relatively integrated with a length of 5~28 cm and an RQD value of 20%-45%. Only a small portion is fragments

The surface water of the slope is not abundant and mainly comes from rainfall. The types of groundwater are the pore water in Quaternary deposits and the fissure water in bedrock. They both are provided by rainfall. However, sandstone, the underlying bedrock, has a weak permeability and belongs to the relative water-resisting strata. Most infiltrated rainwater is stored instantly in Quaternary deposits.

3. Reinforcement Design of the Highway Cut Slope

According to the highway design, the highway pavement is about 24.5 m wide, and the subgrade on this section is designed to form by excavation, and then there will be a cut slope in both sides of the highway, especially the cut slope on the right, where the landslide happened. The slope on the right side is divided into a vertical part and an incline part. In order to meet the slope stability demand, the prestressed anchored sheet piles are designed in the vertical slope; the piles are 35 m long with the space of 5 m along the highway. Three rows of anchors are designed on each pile; their length are 35 m, 30 m, and 25 m from top to toe with the prestress of 15 tons. The diameter of the anchor is 120 mm and each anchor cable has 5 strands with the diameter of 15.2 mm; its elastic module is 1.95×10^8 kPa and the tensile strength is 1.86×10^6 kPa. The inclined slope surface above the pile top is protected with lattice frame construction. The maximal height difference above the pile top is 20 m in the K19+120 profile. Figure 2 shows the reinforcement design layout in the elevation.

As shown in Figure 2, the whole slope can be divided into two parts along the highway mileage. The first section slope is from K19+060 to K19+200, and the second section slope is from K19+200 to K19+320. Figures 3 and 4 represent their typical engineering geology cross-section profile with reinforcement work. The cut slope above the pile top of the first section was excavated into two stages with the ratio of 1.0 : 0.75, and the cross-sectional size of anti-slide piles was 2.0 m × 3.0 m. The slope above the pile top of the second section was excavated in one stage with the ratio of 1.0 : 1.0. The cross-sectional size of anti-slide piles was 2.0 m × 2.4 m. The

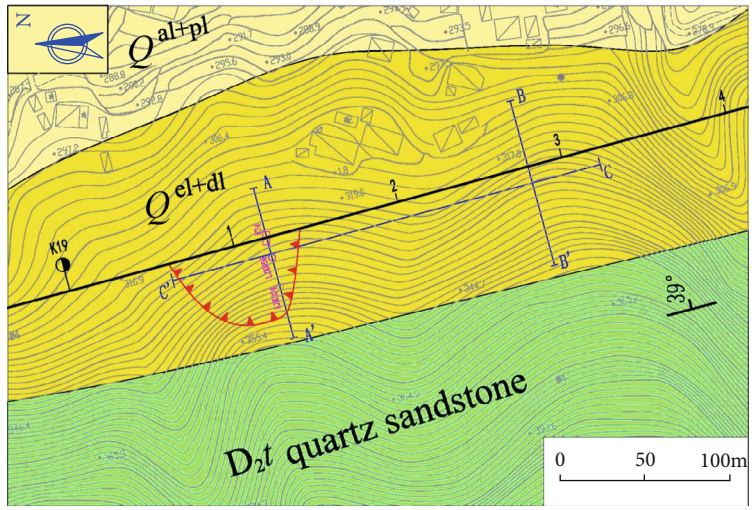

Figure 1: Geological engineering plane.

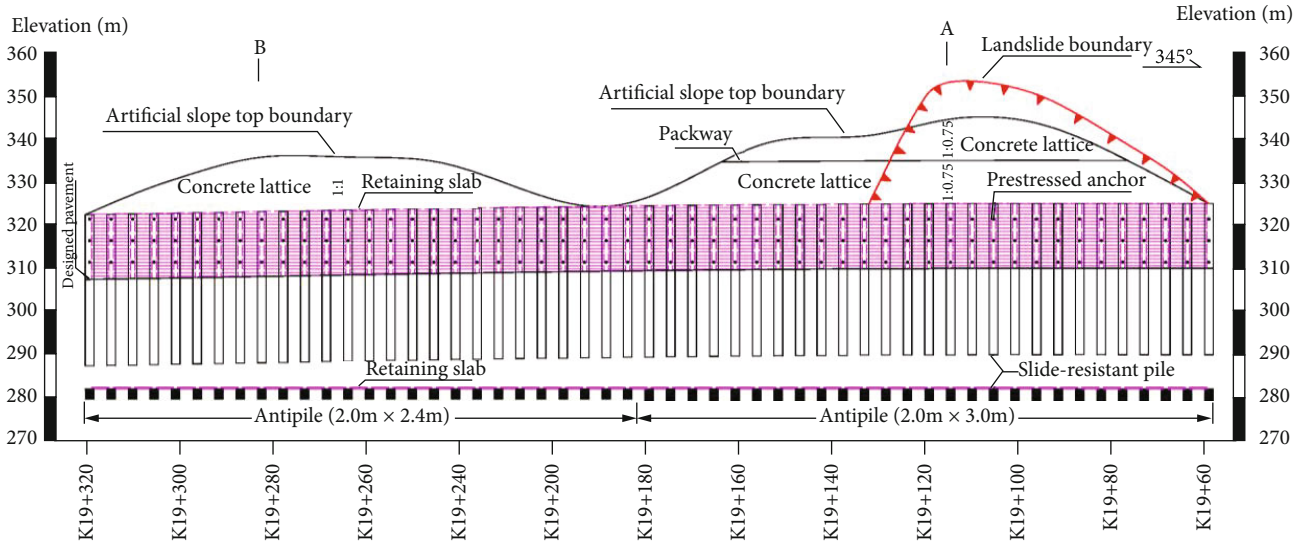

Figure 2: The elevation layout of the reinforcement engineering.

whole slope surface above the pile top is protected by lattice frame constructions and grass planting.

4. Slope Deformation and Influencing Factors

The excavation of the slope began on March 2nd, 2012. Excavation and anti-slide piles were not finished until October 8th, 2012. After continuous rainfall since November 2012, the cut slope on the right side of K19+060~K19+140 failed as a landslide on the morning of November 12th, 2012, as shown in Figure 5.

The landslide is approximately 80.7 m long, 39.8 m wide, and 15.4 m thick, and its sliding direction is towards S35°W. The altitude on the rear of rupture surface is approximately 352.5 m, and that on the toe of the rupture surface is 310.0 m, the same altitude as the pavement. The height difference between the rear and the toe is approximately 42.5 m. The area of this landslide is nearly 2,800 m^2, and the total volume is approximately 23,500 m^3. The landslide is largely composed of gravel soil of Q^{el+dl} and a little weathered siltstone lying in the toe of the landslide, which had been broken into fragments when the slope failed. The majority of the sliding surface is along the interface of gravel soil and siltstone, and it changes to the siltstone layer just in the toe of the landslide. Moreover, before the construction of anchor cables, the constructed anti-slide piles in K19+060~K19+140 had already been destroyed, such that the cantilever of each pile was totally sheared off.

Before the slope failed, there were some intermittent shear cracks on both sides of the slope. According to the survey on November 12th, 2012, the distance from the slope crest to the farthest arc crack was 20 m more than that to the designed intercepting ditch. Most tensile cracks were connected with shear fissures on both sides, and the fissures were less than 15 cm in width and no more than 0.6 m in depth. The vertical displacement of piles on the top was

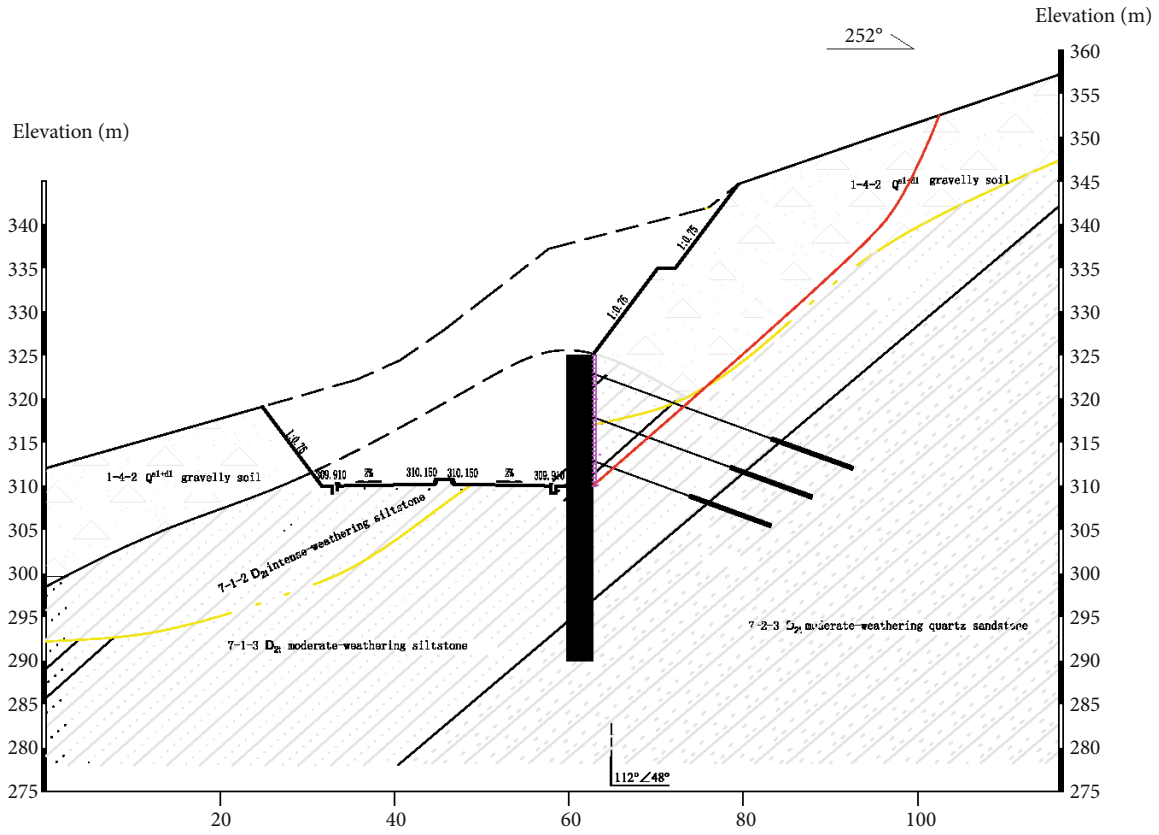

Figure 3: Engineering geology cross-section profile with reinforcement work of the cut slope (A-A').

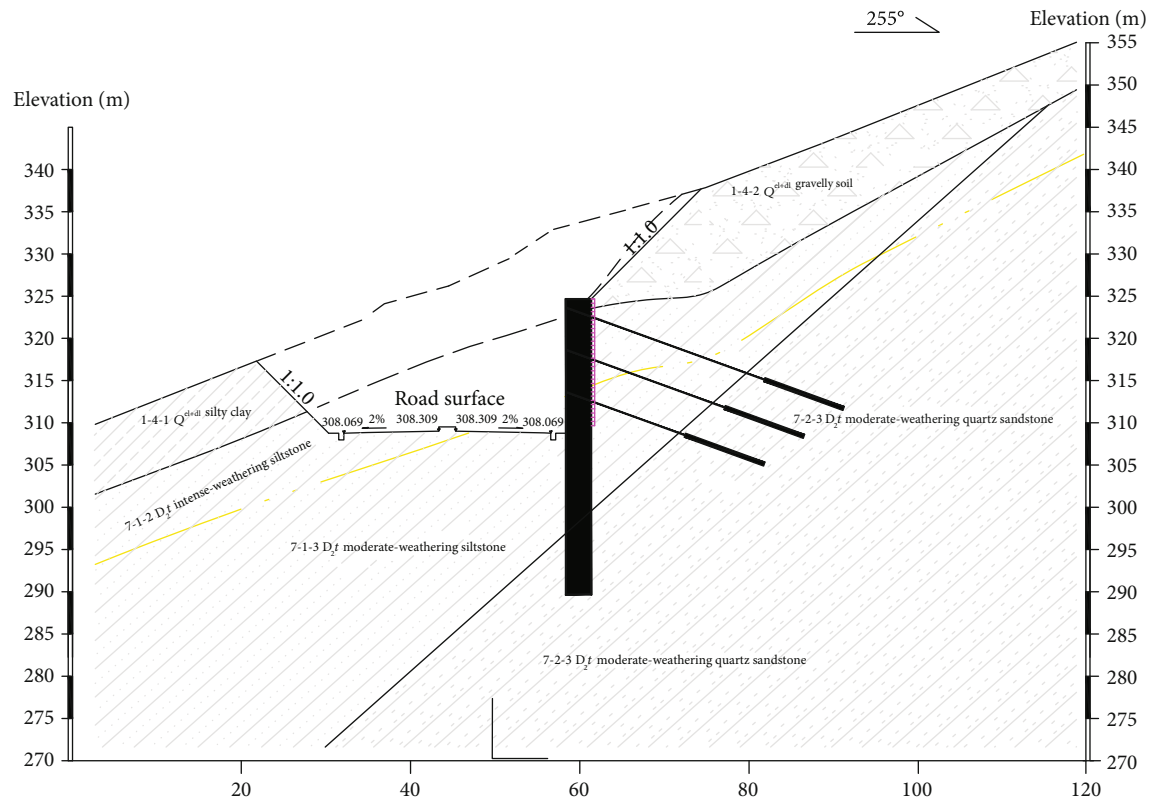

Figure 4: Engineering geology cross-section profile with reinforcement work of the cut slope (B-B').

(a) The damaged slope (b) The sheared antipiles

Figure 5: Photos of the landslide failure.

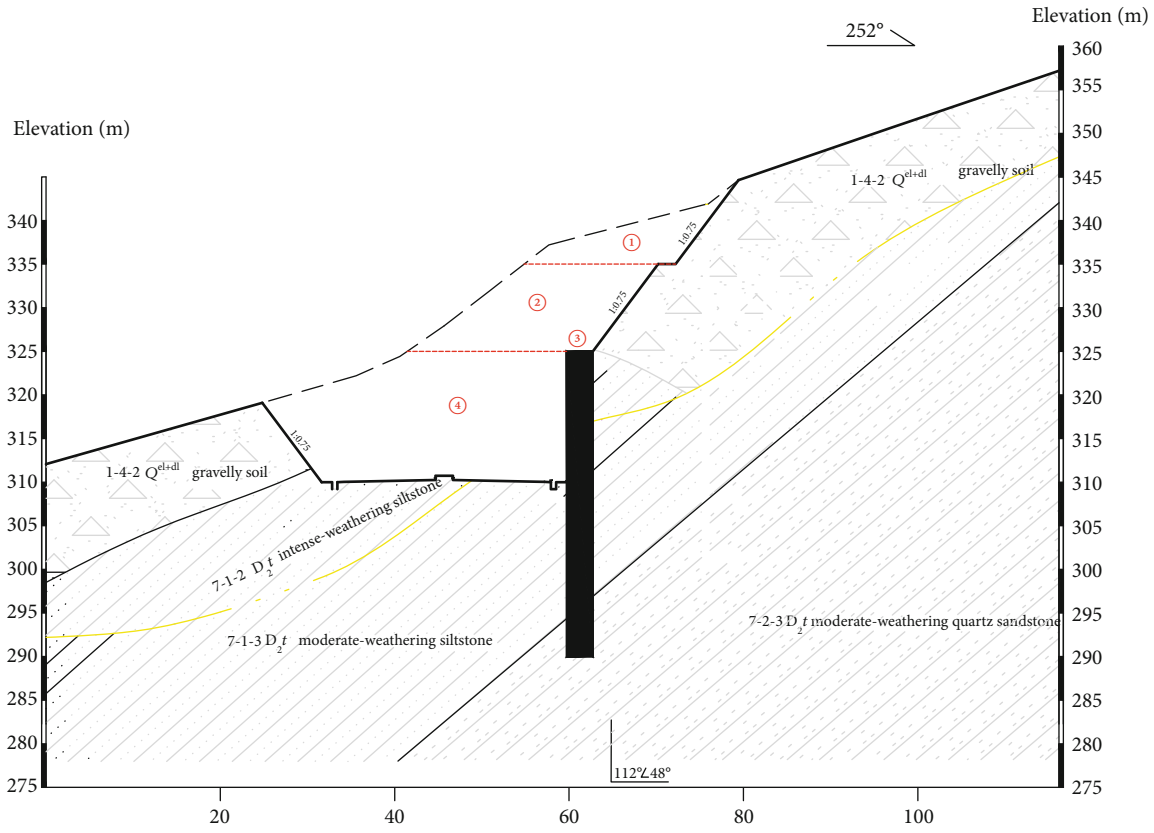

Figure 6: Actual construction steps.

approximately 25 cm, and the gap was 1-7 cm wide. Tensile fractures, distributed in the shape of a crown, were connected to the back scarp.

According to the data investigated and collected and the construction log, we attribute the slope failure to the irrational construction process and rainfall.

4.1. Construction Process. The construction log shows that the actual construction process was run as the following order, as shown in Figure 6:① excavation and protection of the upper slope above the pile tops; ② excavation and protection of the lower slope; ③ construction of the anti-slide piles, in which all were constructed with interval modes by manual excavation; and ④ rock and soil excavation in front of the piles. The slope failed just when the four steps above were finished; the subsequent procedures have not yet been implemented. Each step is reasonable according to the construction log; however, a severe danger is hidden. The design concept should be that the slope would be safe enough to reach the specification requirement when only the prestressed anchor sheet piles are implemented. Therefore, before the anchors and the retaining plates are implemented,

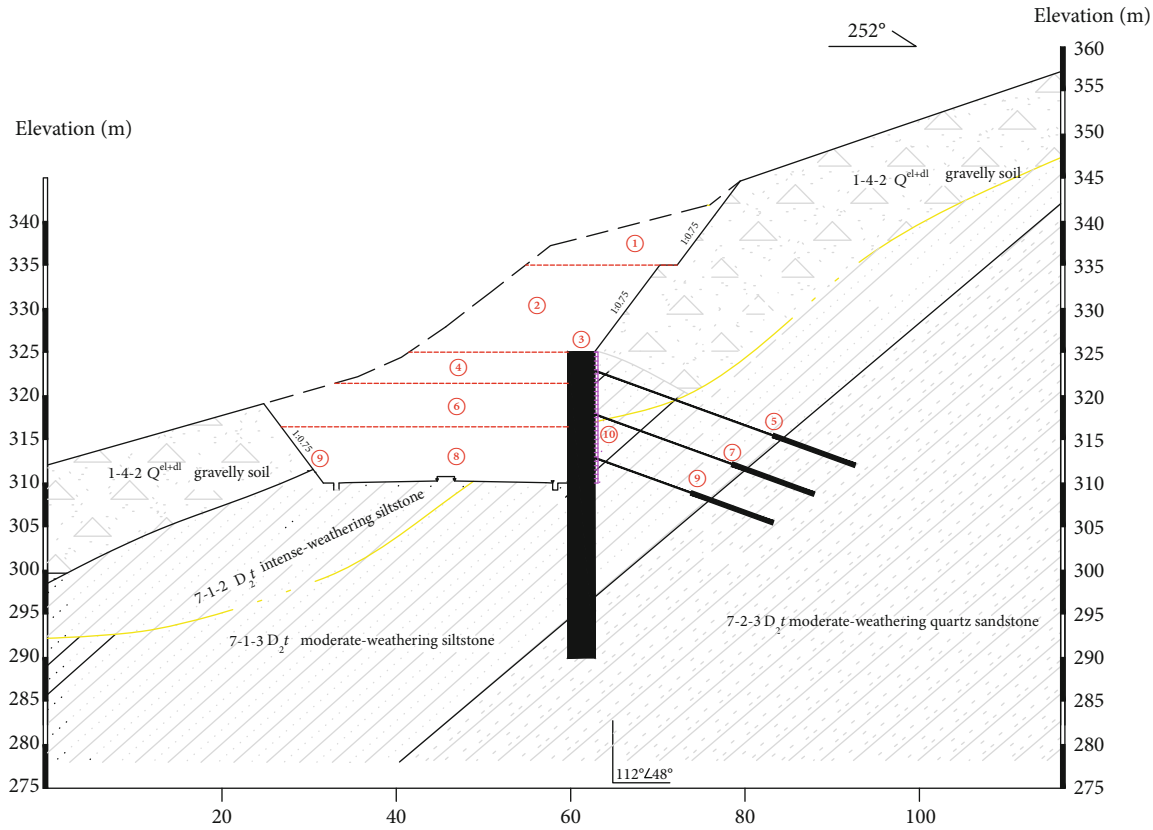

Figure 7: Suggested rational construction steps.

the rock and soil in the front of the anti-slide piles should not be excavated at once as in the fourth step. Obviously, such construction procedures went against the original design intention, which was meant to ensure the slope stability using both anti-slide piles and anchor cables.

The irrational construction process is the key factor causing the slope failure. The actual construction process led to anchor late cable implementation. Here, each anti-slide pile without the anchor turned into a 15-meter-long cantilever pile when the rock mass and soil in front of the piles were excavated. The greatest disadvantage of a cantilever pile is that its displacement is generally bigger than that of an embedded pile. Moreover, retaining plates between the piles had not yet been implemented. All of these would promote the rock and soil behind the piles moving towards the free face, and then the stress condition of the slope adjusted, which is a disadvantage to the stability of the slope. If anchor cables had been implemented in time, the displacement and the stress adjustment of the slope above the top of the anti-slide piles would have been well controlled, and the slope failure would not have happened.

Based on the above analysis, the rational construction process is suggested and shown as Figure 7. The order is as follows: ①–② excavation and protection of the slope above the top of the anti-slide piles, ③ construction of anti-slide piles (steel tubes should be preburied at the position where the anchor cables would be constructed), ④ excavation of the rock and soil above the middle height of the upper two

Table 1: Climate of Yanling County before the landslide.

Date	Maximum temperature (°C)	Minimum temperature (°C)	Weather
2012-11-01	22	7	Sunny
2012-11-02	23	7	Cloudy
2012-11-03	20	10	Cloudy to drizzle
2012-11-04	20	10	Drizzle
2012-11-05	19	8	Cloudy to showers
2012-11-06	22	8	Cloudy
2012-11-07	13	11	Cloudy to drizzle
2012-11-08	15	11	Moderate rain
2012-11-09	13	10	Moderate to heavy rain
2012-11-10	13	11	Light to moderate rain
2012-11-11	14	10	Light rain
2012-11-12	18	8	Cloudy

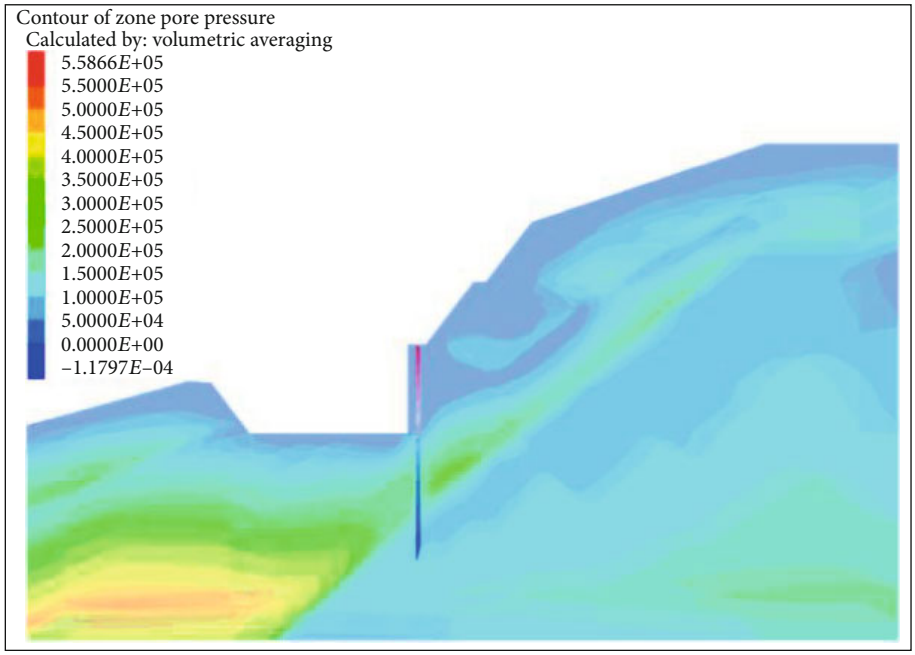

(a) The pore pressure after 1-day rainfall

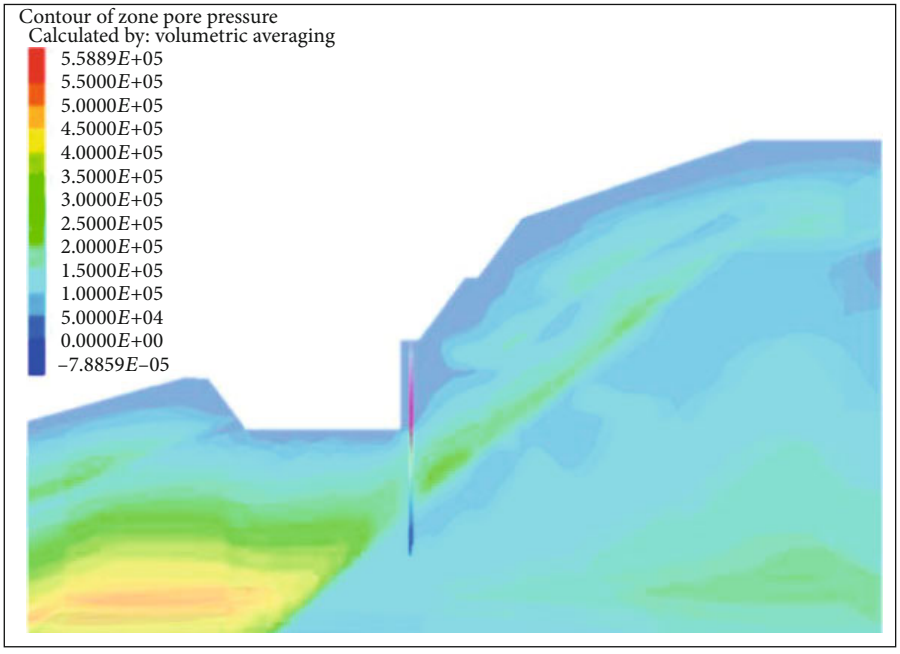

(b) The pore pressure after 3-day rainfall

Figure 8: Continued.

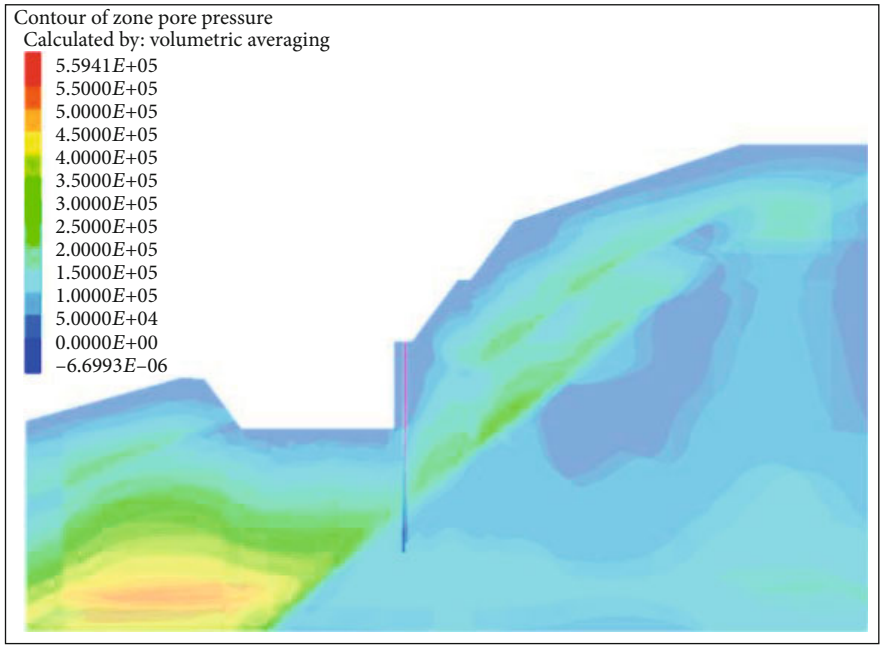

(c) The pore pressure after 5-day rainfall

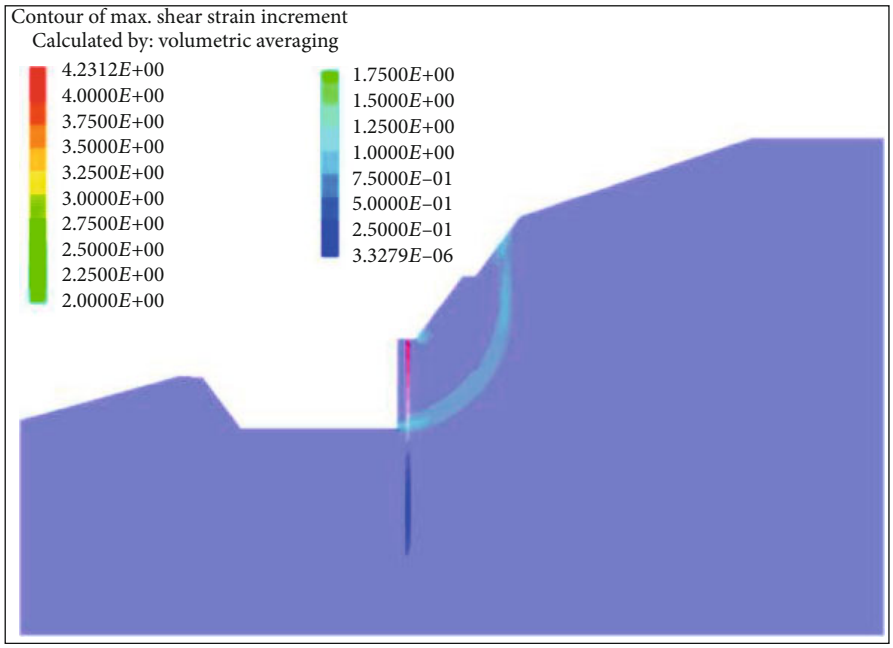

(d) The maximum shear stress increment

Figure 8: Coupled analysis results of the cut slope with the actual construction steps.

rows of anchors, ⑤ construction of the first row of anchors, ⑥ excavation of the rock and soil above the middle height of the following two rows of anchors, ⑦ construction of the middle row anchors, ⑧ excavation of the remaining rock and soil, ⑨ construction of the last row of anchors, and ⑩ installation of prefabricated retaining plates.

4.2. Rainfall. Rainfall is considered as a significant factor. According to the meteorological data in Table 1, it rained 8 of 12 days just before the slope failed. However, according to the supplementary drill holes and an investigation in the landslide, there is no stable groundwater table in the slope. This means that the main effect of rainwater in the slope increases the self-gravity of soil and decreases its shear strength.

The overburden on the slope was composed of silty clay and gravel soil, which have high permeability. The overlaying bedrock is strongly and moderately weathered siltstone. Strongly weathered siltstone has relatively high permeability due to many discontinuities, whereas moderately weathered siltstone is of low permeability. Therefore, the overburden and strongly weathered siltstone become relatively rich water-bearing layers, and the moderately weathered siltstone

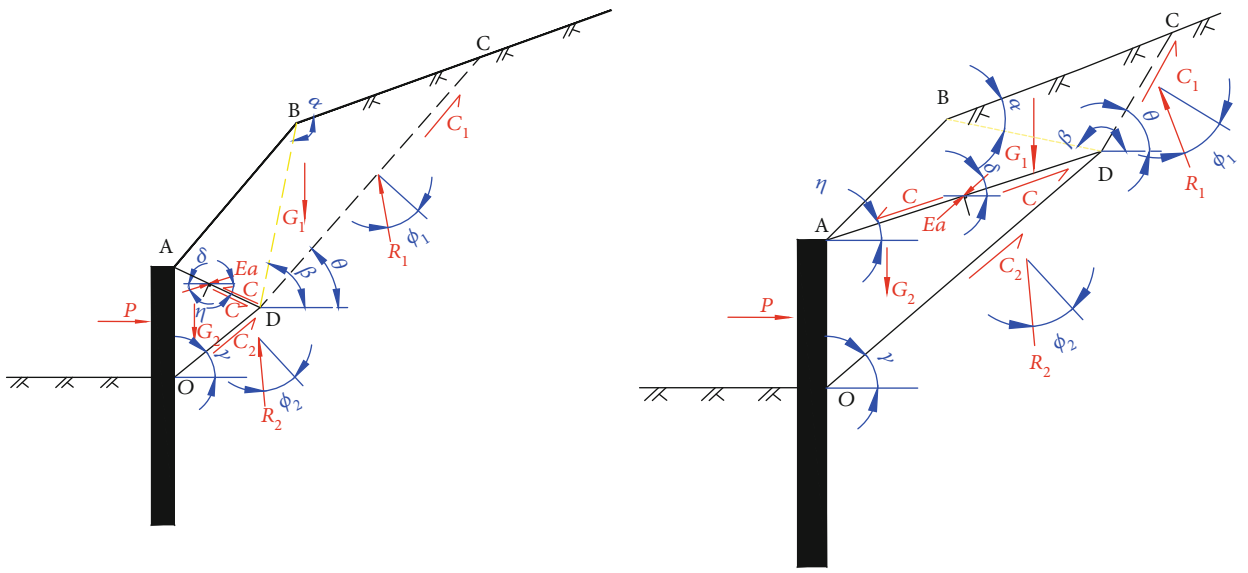

(a) Profile of A-A'

(b) Profile of B-B'

Figure 9: Mechanical analysis of rock mass and soil behind antipiles.

Table 2: Physical and mechanical parameters of rock mass, soil, and materials.

	Density ρ (kg/m^3)	Elastic modulus E (kPa)	Poisson ratio ν	Cohesive C (kPa)	Friction angle ϕ (°)	Hydraulic conductivity k (cm/s)	Porosity p
Gravel soil	21.5	4.9×10^4	0.32	8	32	1.4×10^{-2}	0.28
Strongly weathered siltstone	23.0	5.8×10^6	0.24	35	32	1.2×10^{-5}	0.33
Moderately weathered siltstone	23.4	9.1×10^6	0.20	40	35	1.2×10^{-8}	0.19
Pile	25.0	2.9×10^7	0.13	/	/	/	/

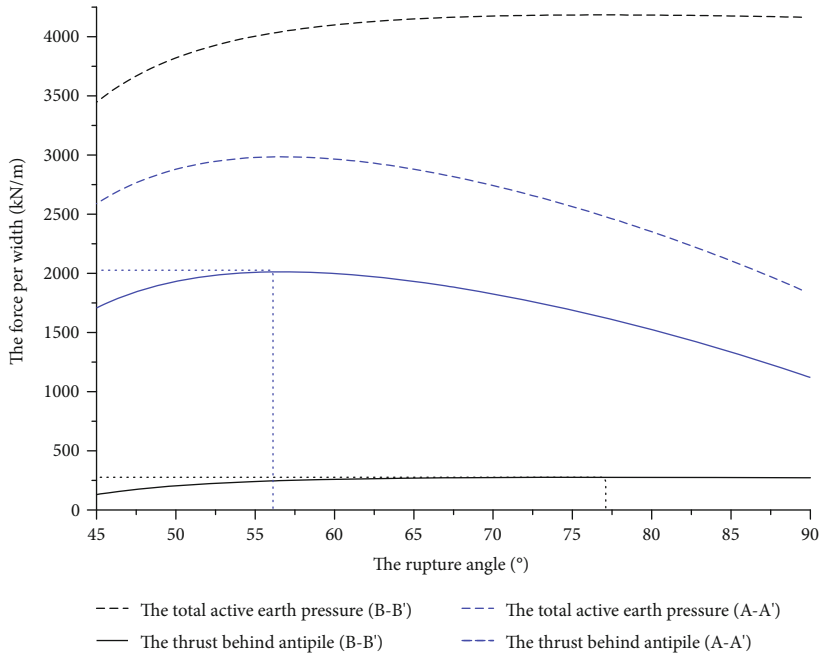

Figure 10: The active earth pressure and the thrust behind the antipiles with different rupture angles.

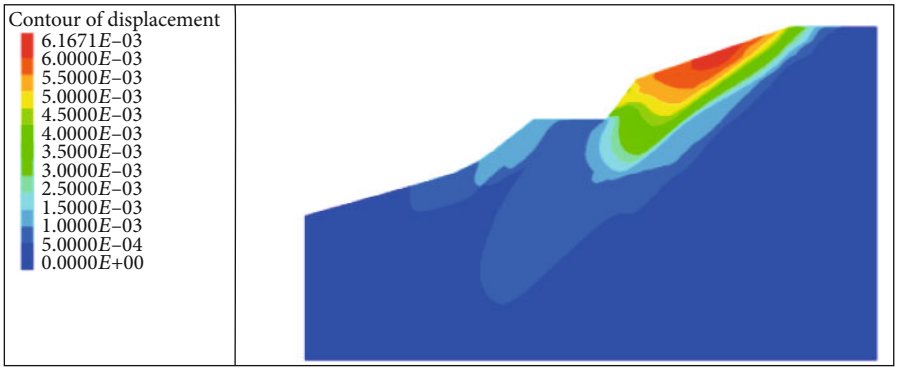

(a) The excavation of the first grade slope

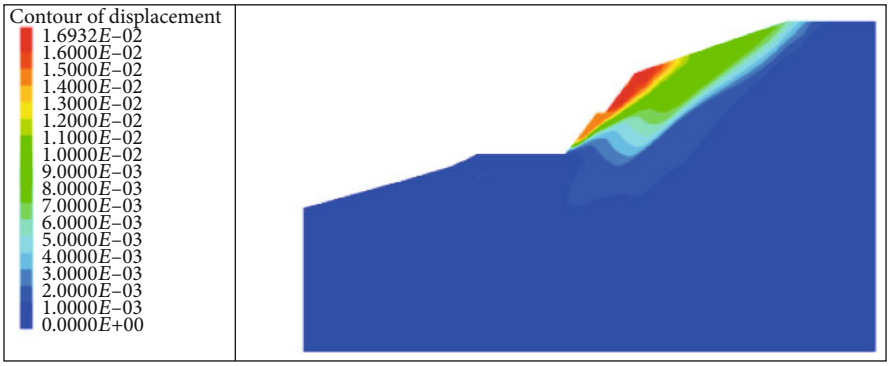

(b) The excavation of the second grade slope

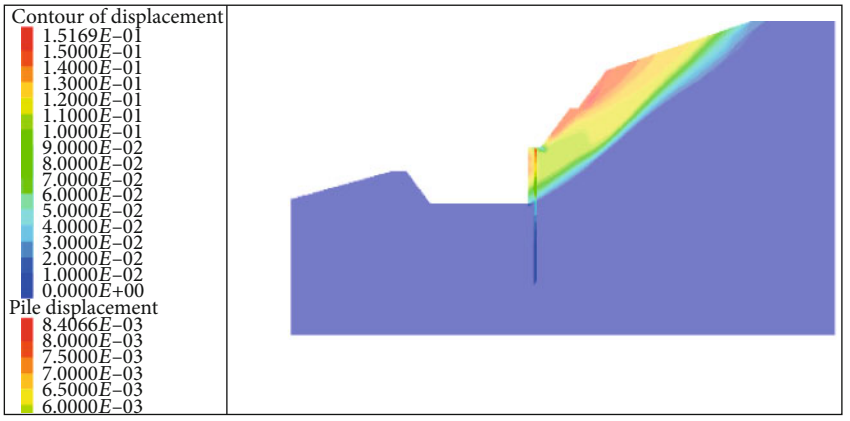

(c) The completed construction

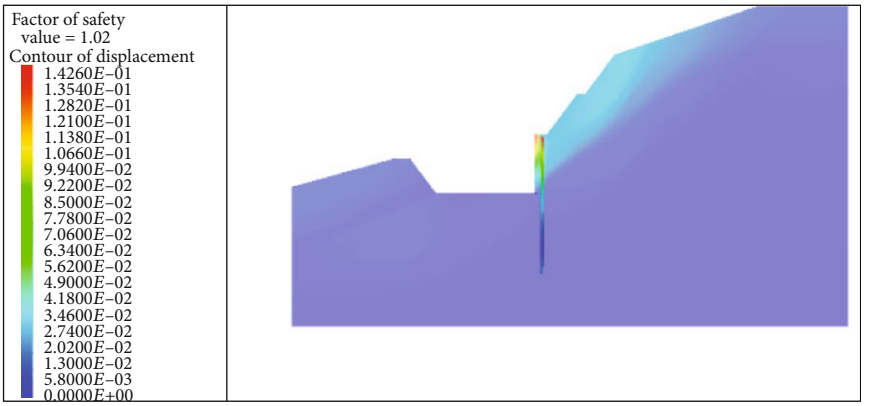

(d) The slope stability when the construction is completed

Figure 11: The displacement simulated from the actual construction process.

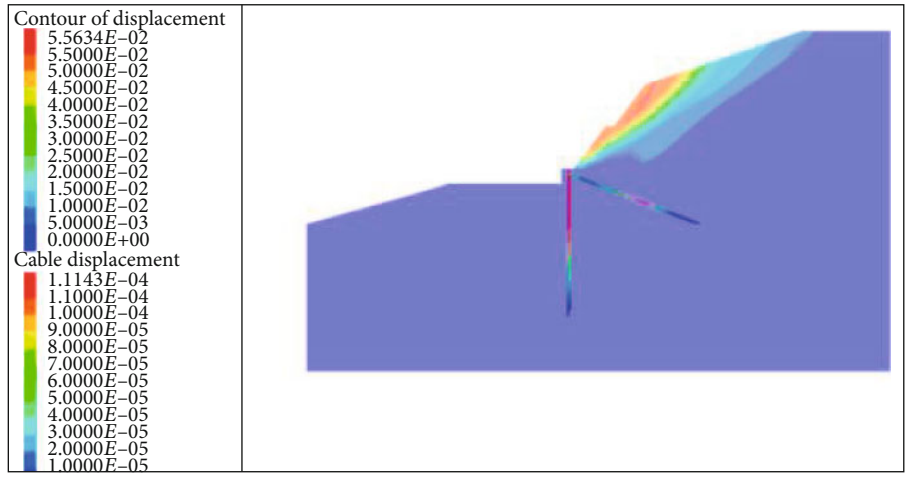

(a) The pile and first row anchor construction

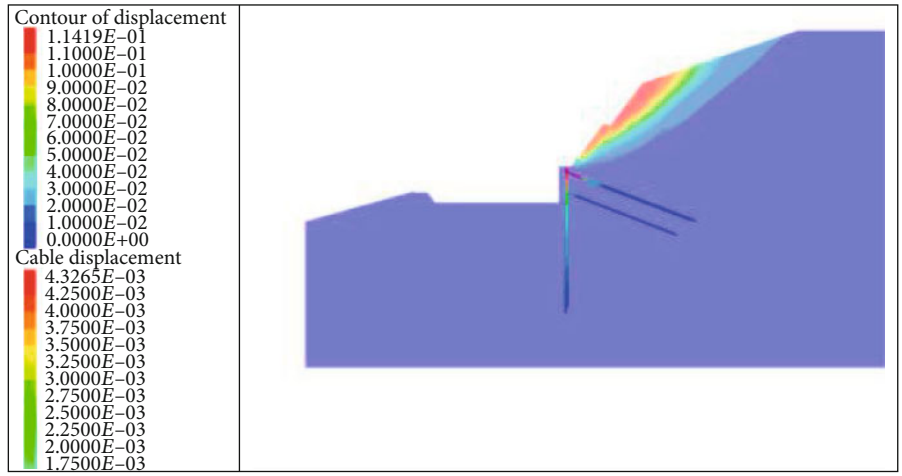

(b) The second row anchor construction

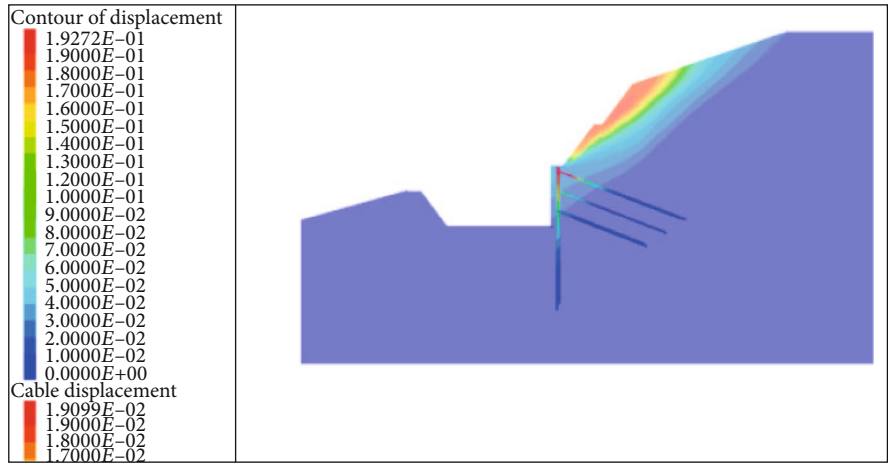

(c) The third row anchor construction

Figure 12: Continued.

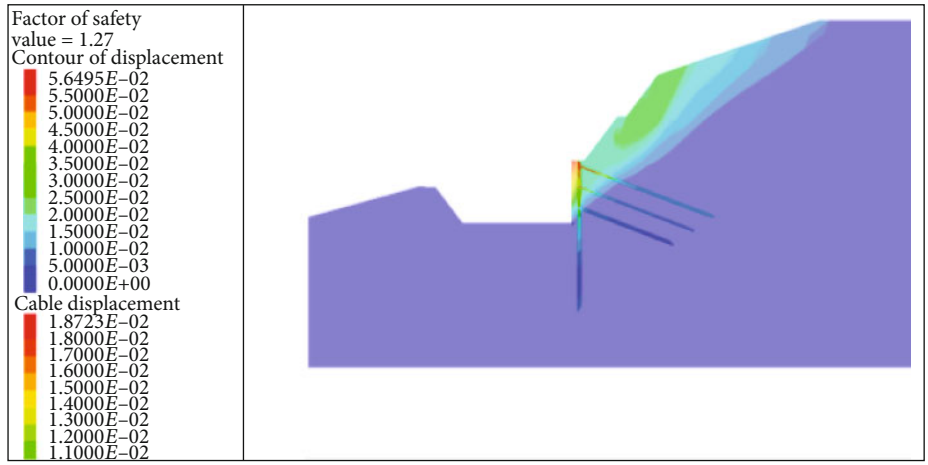

(d) The slope stability when the construction is completed

Figure 12: Numerical simulation of suggested rational construction process.

was a confining bed. Moreover, the cut slope of the highway is a dip slope, which will accelerate the groundwater infiltration in the geological body. Persistent rainfall increased the weight of the slide mass and improved the seepage force as well. The water absorbing capacity of the gravel soil near the interface of soil and siltstone is strong in general, which obviously softens the soil and weakens its shear strength. Therefore, rainfall is another significant factor inducing the slope failure.

Because the failure of the slope is a sudden accident, there is no detailed data about water pore pressure. However, it is known that it rained continuously 5 days before the slope failed according to meteorological records. In order to remedy the lack of the water pore pressure, the seepage of the cut slope was simulated with FLAC^{3D}, and here, the rainfall intensity was considered as 40 mm/day. The distribution of pore water pressure and maximum shear stress increment are given in Figure 8. It shows that the pore water pressure near the slope surface increased continuously during the rainfall process. After 5 days of rainfall, only a small amount of negative pore water pressure exists, and a high saturation area is formed on the face, especially at the toe of the slope. The maximum shear strain increment extends from the top of the third grade slope to the toe of the slope, indicating that the whole slope is a failure.

The landslide occurred in the first section slope, because its stability was worse than that of the second one. The reasons can be summarized as the following: (1) the gravel soil is widely distributed in the first slope, whereas strongly or moderately weathered siltstone is mainly distributed in the middle and front of the second section slope; (2) the altitude difference of the first slope is larger than that of the second; and (3) the slope ratio of the first section slope is greater than that of the second section.

Although the second section slope is currently stable, if it maintains its current state for a long period, the slope would also fail and even induce a new landslide because of rainfall. The mechanical analysis and some numerical simulation would be helpful for us to understand the failure mechanism.

5. Analysis of the Failure Mechanical Mechanism

The slope failure attributes to the irrational construction process and continuous rainfall, their effects can be quantitatively analyzed with static equilibrium functions. Based on Coulomb earth pressure theory, the active earth pressure of this slope can be simplified as shown in Figure 9. Zone ADO represents the siltstone, and zone ABCD represents the gravel soil. The earth pressure acts in the interface AD of gravel soil and siltstone. To simplify calculations, the shear strength of the interface is assumed to be two-thirds as strong as that of gravel soil, and the interface of the anti-slide pile and siltstone is smooth. The lengths of BC and CD would vary with the change of the angle θ.

According to the static equilibrium of part ABCD and part ADO, the following formulas can be obtained:

$$\begin{cases} (C_1 + R_1 \sin \phi_1) \cos \theta + C \cos \eta + E_a \cos \delta = R_1 \cos \phi_1 \sin \theta, \\ G_1 + C \sin \eta - E_a \sin \delta = (C_1 + R_1 \sin \phi_1) \sin \theta + R_1 \cos \phi_1 \cos \theta, \end{cases} \tag{1}$$

$$\begin{cases} P + (C_2 + R_2 \sin \phi_2) \cos \gamma = E_a \cos \delta + R_2 \cos \phi_2 \sin \gamma + C \cos \eta, \\ R_2 \cos \phi_2 \cos \gamma + (C_2 + R_2 \sin \phi_2) \sin \gamma + C \sin \eta = G_2 + E_a \sin \delta, \end{cases} \tag{2}$$

where G_1 and G_2 are the weights of parts ABCD and ADO, respectively, kN; C_1, C_2, and C denote the tangential forces caused by the interface cohesion as shown in Figure 9, kN; and R_1 and R_2 denote the forces on the interface contributed by the friction angle, kN. E_a is the active earth pressure on the interface of parts ABCD and ADO, kN. P is the force between pile and soil, kN. ϕ_1 and ϕ_2 are the cohesive of the rupture surface on parts ABCD and ADO, respectively, °. θ, γ, and η are the tilt angles of rupture surfaces CD, DO, and AD, °.

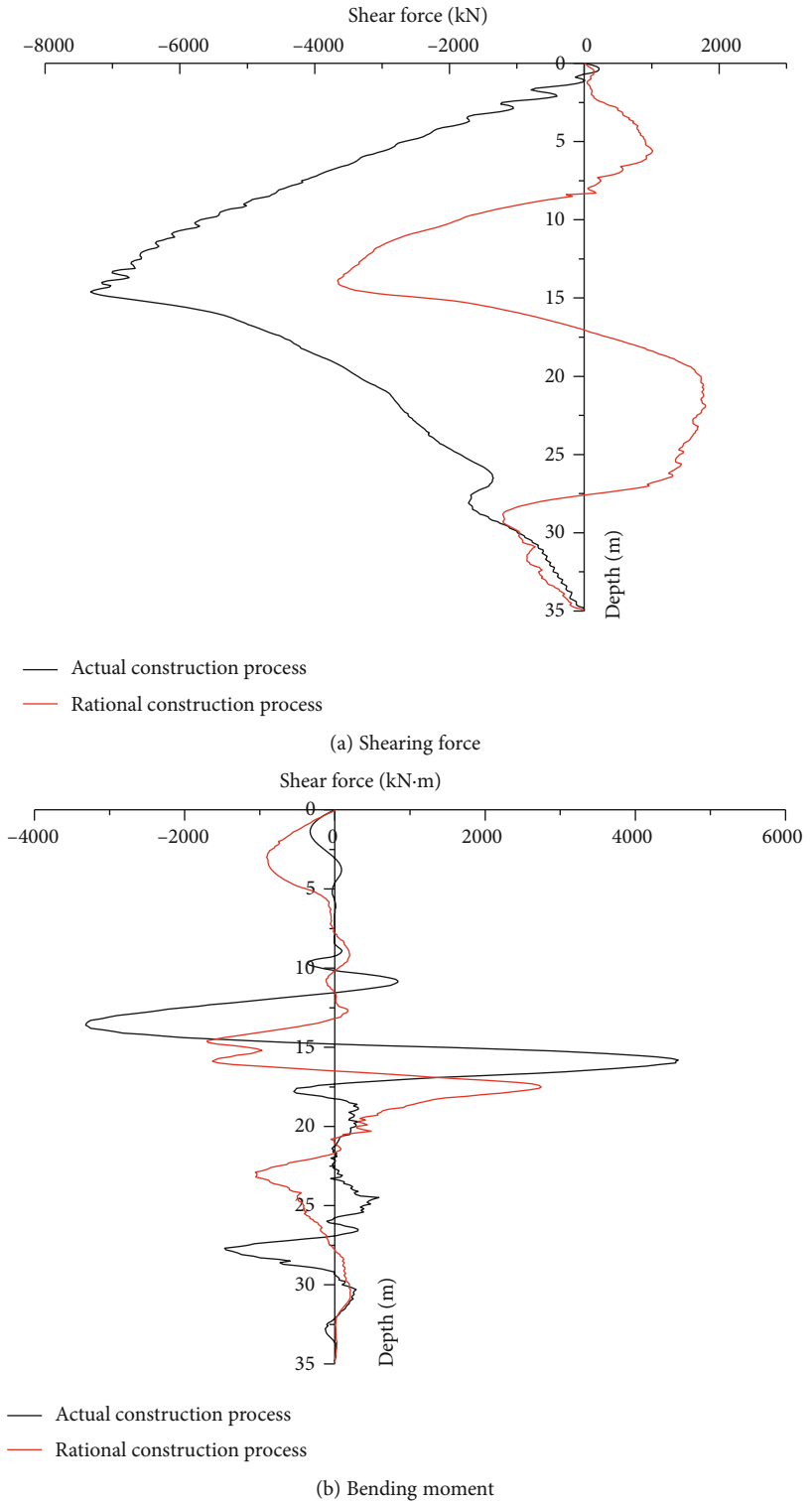

Figure 13: The internal force simulated from two different construction processes.

δ is the included angle of active earth pressure with the interface surface AD, °. Then, E_a and P can be deduced, respectively.

$$E_a = \frac{G_1 \sin(\theta - \phi_1) - C\cos(\eta + \theta - \phi_1) - C_1 \cos\phi_1}{\cos(\delta - \theta + \phi_1)}, \quad (3)$$

$$P = \frac{G_2 \sin(\gamma - \phi_2) + E_a \cos(\delta - \gamma + \phi_2) + C\cos(\eta + \gamma - \phi_2) - C_2 \cos\phi_2}{\cos(\gamma - \phi_2)}. \quad (4)$$

The active earth pressure will increase when it rains. Using the wax seal method and the direct shear box test in the lab, the

saturation density and shear strength parameters of gravel soil, strongly weathered siltstone, and moderately weathered siltstone are gained as shown in Table 2. The rupture angle θ in formula (2) is unknown, and it is assumed that the maximum active earth pressure E_a would be obtained when θ equals the value of θ_0. The mechanical model of the first section slope is shown in Figure 8(a) based on the typical profile A-A'. Here, AD = 12.92 m, BD = 25.59 m, OD = 15.05 m, $S_{\Delta AOD} = 87.92$ m^2, $S_{\Delta ABD} = 160.79$ m^2, and $\alpha = 121°$, $\beta = 79°$, $\gamma = 39°$, $\delta = 65° - \varphi_1$, and $\eta = 25°$. The mechanical model of the second section slope is also shown in Figure 8(b) based on the typical profile B-B'. Here, AD = 31.12 m, BD = 16.96 m, OD = 39.22 m, $S_{\Delta AOD} = 234.99$ m^2, $S_{\Delta ABD} = 130.37$ m^2, and $\alpha = 32°$, $\beta = 168°$, $\gamma = 41°$, $\delta = 106° - \phi_1$, and $\eta = -18°$.

According to Equations (3) and (4), we can calculate the total active earth pressure and the thrust behind the piles under the assumption of different rupture angles. The result is shown in Figure 10. For the first section slope, the maximum active earth pressure per unit width is 2984.84 kN, and the thrust per unit width is 2013.19 kN when the rupture angle $\theta_0 = 56.75°$. For the second section slope, the maximum active earth pressure per unit width is 4184.29 kN, and the thrust per unit width is 275.83 kN when the rupture angle $\theta_0 = 77.0°$.

It shows rock mass between anti-slide piles, and soil in the second section slope eliminates the vast majority of active earth pressure, and then the thrust behind the piles of the second section slope is much smaller than that of the first section. The distance of the adjacent piles is 5 m, so the thrust on each pile of the first section slope should be 10065.97 kN, whereas it is only 1379.16 kN in the second section. Obviously, the first section slope is more dangerous than the second section, which is the mechanical reason of the cut slope failure.

6. Numerical Simulation Analysis

FLAC^{3D} is used to simulate the deformation and stability of the cut slope. The calculation results of the actual and rational construction processes are shown in Figures 11 and 12, respectively. Here, it should be pointed out that the first two steps of the two construction processes are the same; the difference just begins from the third step. Therefore, only the first two steps are given in Figures 11 and 12 which show just the following construction processes. According to the numerical simulation, the slope stability coefficient is 1.02 under the actual construction process and 1.27 under the rational construction process. Under the rational construction process, the anchor cables restrain effectively the deformation of rock and soil behind the piles, reducing the overall displacement of the slope. Therefore, rational construction process can effectively enhance the stability of the slope.

The internal force simulated from the two construction processes is shown in Figure 13. The internal force curves simulated are a little volatile, especially the bending moment. It may be caused by the spatial difference of strata. By comparing the shearing forces and bending moments of the two construction processes, it shows that (1) No matter which construction process, the maximum internal force of the anti-slide pile is distributed near the slope toe. (2) The anchor cables reduce effectively the maximum internal force of the anti-slide pile and improve the internal force distribution of the pile. Furthermore, the shearing force of the rational construction process is decreased to the half of the actual construction process, and the bending moment almost drops down to the three-fifths. (3) The excessive internal force of the pile near the slope toe in the actual construction process is the mechanical mechanism of the cut slope failure.

7. Conclusions

A landslide caused by a cut slope in a highway is taken as an example, and the failure factors are analyzed. Based on the mechanical derivation and numerical simulation, the damage mechanisms are revealed. Some findings are obtained as the follows:

(1) The main reasons of the cut slope failure are the irrational construction process and rainfall. The irrational construction process removed the geological body in front of the anti-slide piles before the anchors were loaded. The designed prestressed anchor sheet piles then turned into the cantilever piles, which could not provide enough resistance to withstand the slope thrust. Furthermore, the surface water infiltrated into the gravel soil because of continuous rainfall. It increased the weight of geological body and weakened the shear strength of the rock and soil

(2) Therefore, after the soil behind the pile creates a certain amount of displacement, the active earth pressure behind the piles and the shearing force and bending moment along the piles increased, which resulted in the damage of the piles and the slope

(3) The mechanical analysis shows that the thrust of the second slope was larger than that of the first one. However, the rock mass behind the piles of the second slope resists a large proportion of the active earth pressure, while the thrust on the piles of the first slope was larger than that of the second slope

Data Availability

The data are available and explained in this article; readers can access the data supporting the conclusions of this study. Figure 5 is composed of photos; Figures 8, 11, and 12 are calculated by FLAC soft. So the figures are not a vectorgraph type.

Conflicts of Interest

The authors declare that they have no conflicts of interest.

Acknowledgments

This work was supported by the National Natural Science Foundation of China (No. 41877263), the Science and Technology Project of Huaneng Lancang River Hydropower Inc. (No. HNKJ18-H24), and the Fundamental Research Funds for the Central Universities, China University of Geosciences, Wuhan (No. CUGCJ1802).

References

[1] F. Ardizzone, M. Rossi, F. Calò et al., "Preliminary analysis of a correlation between ground deformations and rainfall: the Ivancich landslide, central Italy," in *SAR Image Analysis, Modeling, and Techniques XI*, Prague, Czech Republic, 2011.

[2] H. Y. Deng and J. M. Kong, "Spatiotemporal distribution characteristics of reservoir bank landslide deformation driven by rainfall," *Journal of Natural Disasters*, vol. 21, no. 1, pp. 148–154, 2012.

[3] Q. L. Deng, Z. Y. Zhu, Z. Q. Cui, and X. P. Wang, "Mass rock creep and landsliding on the Huangtupo slope in the reservoir area of the Three Gorges Project, Yangtze River, China," *Engineering Geology*, vol. 58, no. 1, pp. 67–83, 2000.

[4] Y. A. Fa, J. M. Kong, and Z. Q. Ni, "Performance enhancement of MBR operated with aerobic granules on membrane filterability improvement," *Disaster Advances*, vol. 43, no. 1-3, pp. 323–331, 2012.

[5] T. Zhang, E. C. Yan, and J. T. Cheng, "Mechanism of reservoir water in the deformation of Hefeng landslide," *Journal of Earth Science*, vol. 21, no. 6, pp. 870–875, 2010.

[6] USGS, 2011, http://landslides.usgs.gov/research/other/centralamerica.php#update1.

[7] Z. Arbanas, S. Dugonjic, M. Vivoda, and V. Jagodnik, "Landslide affected with an open pit excavation in flysch deposit," in *Proceedings of the 15th European Conference on Soil Mechanics and Geotechnical Engineering*, pp. 1319–1324, Athens, Greece, 2011.

[8] T. D. Stark, W. D. Arellano, R. P. Hillman, R. M. Hughes, N. Joyal, and D. Hillebrandt, "Effect of toe excavation on a deep bedrock landslide," *Journal of Performance of Constructed Facilities*, vol. 19, no. 3, pp. 244–255, 2005.

[9] H. W. Zhu, L. K. Yao, L. W. Jiang, and Y. L. Qiu, "Distribution of seismic earth pressure on gravity retaining walls considering influence of deformation," *Chinese Journal of Geotechnical Engineering*, vol. 35, no. 5, pp. 1035–1044, 2013.

[10] S. J. Harris, R. P. Orense, and K. Itoh, "Field monitoring of a highway cut slope for rain-induced instability," in *6th International Conference on Unsaturated Soils*, pp. 1507–1513, Sydney, Australia, 2014.

[11] X. Z. Chen and Y. F. Cui, "The formation of the Wulipo landslide and the resulting debris flow in Dujiangyan city, China," *Journal of Mountain Science*, vol. 14, no. 6, pp. 1100–1112, 2017.

[12] A. S. Chatra, G. R. Dodagoudar, and V. B. Maji, "Numerical modelling of rainfall effects on the stability of soil slopes," *International Journal of Geotechnical Engineering*, vol. 13, no. 5, pp. 425–437, 2017.

[13] S. Zhang, X. C. Zhang, X. J. Pei et al., "Model test study on the hydrological mechanisms and early warning thresholds for loess fill slope failure induced by rainfall," *Engineering Geology*, vol. 258, p. 105135, 2019.

[14] P. K. Singh, A. Kainthola, and S. Prasad, "Protection measures on the failed cut-slope along the free expressway, Chembur, Mumbai, India," *Journal Of The Geological Society Of India*, vol. 86, no. 6, pp. 687–695, 2015.

[15] S. Oh and N. Lu, "Slope stability analysis under unsaturated conditions: case studies of rainfall-induced failure of cut slopes," *Engineering Geology*, vol. 184, pp. 96–103, 2015.

[16] S. Da, O. Taciano, R. C. Nascimento, F. Souza, and W. Jhonatan, "Soil susceptibility to accelerated hydric erosion: geotechnical evaluation of cut slopes in residual soil profiles," *Acta Scientiarum Technology*, vol. 37, no. 4, pp. 331–337, 2015.

[17] A. Kainthola, P. K. Singh, and T. N. Singh, "Stability investigation of road cut slope in basaltic rockmass, Mahabaleshwar, India," *Geoscience Frontiers*, vol. 6, no. 6, pp. 837–845, 2015.